Mon. Not. R. Astron. Soc. **000**, 1–14 (2002) Printed 4 February 2009 (MN LATEX style file v2.2)

New Faint Optical Spectrophotometric Standards. Hot White Dwarfs from the Sloan Digital Sky Survey

Carlos Allende Prieto[1⋆], Ivan Hubeny[2] and J. Allyn Smith[3]
[1] *Mullard Space Science Laboratory, University College London, Holmbury St Mary, Dorking, Surrey RH5 6NT, UK*
[2] *Department of Astronomy and Steward Observatory, University of Arizona, Tucson, AZ 85721, USA*
[3] *Department of Physics and Astronomy, Austin Peay State University, P.O. Box 4608, Clarksville, TN 37044, USA*

Submitted on February 2009

ABSTRACT
The spectral energy distributions for pure-hydrogen (DA) hot white dwarfs can be accurately predicted by model atmospheres. This makes it possible to define spectrophotometric calibrators by scaling the theoretical spectral shapes with broad-band photometric observations – a strategy successfully exploited for the spectrographs onboard the Hubble Space Telescope (HST) using three primary DA standards. Absolute fluxes for non-DA secondary standards, introduced to increase the density of calibrators in the sky, need to be referred to the primary standards, but a far better solution would be to employ a network of DA stars scattered throughout the sky. We search for blue objects in the sixth data release of the Sloan Digital Sky Survey (SDSS) and fit DA model fluxes to identify suitable candidates. Reddening needs to be considered in the analysis of the hottest and therefore more distant stars. We propose a list of nine pure-hydrogen white dwarfs with absolute fluxes with estimated uncertainties below 3 %, including four objects with estimated errors < 2 %, as candidates for spectrophotometric standards in the range $14 < g < 18$, and provide model-based fluxes scaled to match the SDSS broad-band fluxes for each. We apply the same method to the three HST DA standards, linking the zero point of their absolute fluxes to *ugr* magnitudes transformed from photometry obtained with the USNO 1-m telescope. For these stars we estimate uncertainties of < 1 % in the optical, finding good consistency with the fluxes adopted for HST calibration.

Key words: techniques: spectroscopic – catalogues – white dwarfs – stars: fundamental parameters.

1 INTRODUCTION

Good flux standards are hard to get. Ground-based observations are limited in accuracy by time-dependent variations in transparency of the terrestrial atmosphere. Spaced-based fluxes are free from atmospheric distortions, but are more difficult to relate to standard sources in the laboratory. In addition, charge-transfer efficiency problems in CCDs become more acute in space due to bombardment by high-energy particles. Despite these issues, the Hubble Space Telescope CALSPEC spectrophotometric standards, advertised to provide absolute fluxes good to about 1-2 % in the optical and near-infrared, constitute the preferred reference.

The CALSPEC absolute fluxes are based on model atmospheres for three hot DA white dwarfs normalized to Landolt V-band photometry (Bohlin 1996, 2000; Bohlin, Dickinson & Calzetti 2001). In this calibration, the spectral energy distribution postulated for these stars is computed with hydrostatic plane-parallel NLTE pure-hydrogen model atmospheres calculated with the code Tlusty (see §2). These atmospheres consist of hydrogen and free electrons, and are free from convection. Under the assumption that the physics of DA atmospheres is well-known, these objects are then promoted to space calibration sources (see, e.g., Holberg et al. 1982, 1991; Finley, Basri & Bowyer 1990; Bohlin, Colina & Finley 1995; Kruk et al. 1999; Sing, Holberg & Dupuis 2002; Liebert, Bergeron & Holberg 2005; Dixon et al. 2007). Comparison with trigonometric parallaxes available for the brightest DA white dwarfs gives empirical support to this procedure (Holberg, Bergeron & Gianninas 2008).

Fitting intermediate-resolution spectra of these stars provides estimates of the two parameters that define their atmospheric models, effective temperature and surface gravity, with a precision better than ~ 1% and 0.1 dex, respectively. These uncertainties influence the predicted spectral energy distribution to a level of < 1 % throughout the opti-

⋆ E-mail: cap@mssl.ucl.ac.uk

cal and near-infrared. The solidity of the theoretically predicted relative fluxes can be appraised by comparing calculations with independent codes. For an effective temperature of 20,000 K, LTE models computed by Koester (e.g., Kilic et al. 2007) predict continuum spectra that deviate from Tlusty's by only 0.5 % in the optical and near-infrared, and the differences reach only 1% at 30,000 K, due in part to departures from Local Thermodynamical Equilibrium (LTE), as illustrates Fig. 1.

DA white dwarfs are ideal calibration sources for other reasons. They are intrinsically faint, and therefore located at small distances, which renders their observed fluxes unaffected by interstellar extinction. Comparatively, B- and A-type stars, also with relatively smooth continua dominated in the optical and near-infrared by bound-free hydrogen opacity, present several disadvantages. They show weak metal lines, are located at larger distances from Earth, and some are surrounded by disks (Laureijs et al. 2002), which might disturb their spectral shapes in the infrared. Furthermore, many early type stars rotate fast (see the example of Vega; Adelman & Gulliver 1990) and, although this is hard to detect in the spectrum when the rotational axis is aligned with the line of sight, rotation can distort significantly their spectral energy distribution and broad-band colors (Pérez Hernández et al. 1999, Aufdenberg et al. 2006).

F-type subdwarfs such as the SDSS standard (BD +17 4718; Bohlin & Gilliland 2004; Ramírez et al. 2006) are abundant in the turn-off of the Galactic halo and thick-disk populations, but again, they are located at considerably larger distances, and their continua are influenced by both hydrogen and H^- photoionisation, with the contribution of the latter varying depending on the number of free electrons available, which makes their spectral shape dependent on their exact metal abundance, increasing the complexity of the model atmosphere calculations.

In addition to the three fundamental DA stars that set the CALSPEC absolute fluxes, Hubble Space Telescope (HST) spectrophotometry links observations of other stars (some of which are DA) to the fundamental standards, expanding the calibration network to about two dozen objects throughout the sky. This is important, as three standards are not enough for accurate calibrations, in particular for ground-based observations where small angular separations between target and calibrator are a must. Nonetheless, this two-step process may result in a loss of accuracy and, due to the miscellaneous nature of the secondary calibrators and the resulting large range in distance and extinction, significant variations in quality across the sky.

The link between the secondary HST flux standards and the three primary ones depends on the calibration of the time-dependent response of the HST spectrographs. The risk of using secondary standards is nowhere more evident than in the recent update of Vega's HST spectrophotometry. After considering charge transfer efficiency corrections for the STIS CCD (see Goudfrooij et al. 2006), the slope in the Paschen continuum was modified by about 2%. Such a change implies a decrease in the inferred effective temperature from 9550 K to 9400 K (Bohlin 2007), and in fact, it solves a long-standing discrepancy between the HST and the IUE-INES flux scales (García-Gil et al. 2005).

Instead of using secondary standards, based themselves of observations that are ultimately tied to the three white dwarfs chosen by Bohlin and collaborators, the flux scale can be set in a single step using a larger number of well-behaved pure-hydrogen hot white dwarfs. But those must be first identified.

The Sloan Digital Sky survey is a major source of large numbers of DA white dwarfs in the range $14 < V < 21$ (Harris et al. 2003, Kleinman et al. 2004, Eisenstein et al. 2006). In this work, we use spectra and photometry in the sixth data release (Adelman-McCarthy et al. 2008) to identify hot DA stars, deriving a homogeneous set of atmospheric parameters and absolute fluxes for them to propose an expanded network of DA primary standards. Section 2 elaborates on our analysis procedure. Section 3 describes our sample and the results. Section 4 describes the determination of the zero points of the absolute flux scale, and in §5 we present our standard candidates. Section 6 revisits the determination of atmospheric parameters for the HST primary standards, and §7 closes the paper with a brief summary.

2 ANALYSIS

We focus on DA stars with a surface temperature warmer than 20,000 K. This avoids known problems with models for DA cooler than about 12,000 K for which unexpectedly large surface gravities are derived from the analysis of Balmer lines (see, e.g. Bergeron, Saffer & Liebert 1992, Eisenstein et al. 2006). Our choice of temperatures avoids the presence of significant convective energy transport in these atmospheres, allowing us to safely assume radiative balance.

We use an unpublished grid of model fluxes for DA stars previously calculated by Hubeny. The model atmospheres contain only hydrogen and are computed, in Non-LTE, with the code Tlusty (Hubeny & Lanz 1995, Lanz & Hubeny 1995). The code, and the hydrogen model atom used are publicly available from the Tlusty web site[1]. We considered surface gravities in the range $7 < \log g < 9.5$ (c.g.s. units). Among the most important ingredients, H line profiles were calculated with the Stark broadening tables of Lemke (1997), and the level dissolution, occupation probabilities, and the pseudo-continuum opacities were taken from Hubeny, Hummer & Lanz (1994).

Our spectral analysis uses the same code and principles outlined in Kilic et al. (2007), but we have added one more dimension to the problem in order to account for reddening. For each star we determine the trio $(T_{\rm eff}, \log g, E(B-V))$ of a model that matches best the observations in the region $385 - 540$ nm (air wavelengths). The spectra are either normalized by a constant, taken as the median value of the flux in the selected spectral window, or by a polynomial model of the star's pseudocontinuum (see §3 for more details). A wavelength grid equidistant in $\log\lambda$ was employed. The theoretical fluxes are computed for a discrete grid with steps of 2,000 K and 0.5 dex for $T_{\rm eff}$ and $\log g$, respectively, and smoothed to a FWHM ($\equiv \delta\lambda$) resolving power of $\lambda/\delta\lambda = 2000$, which approximately corresponds to that of the SDSS spectra. Reddening is introduced with a discrete grid sampling $0 < E(B-V) < 0.095$ in steps of

[1] `http://nova.astro.umd.edu`

Table 1. Parameters derived from SDSS spectra.

Name	SDSS spectrum	$T_{\rm eff}$ (K)	$\log g$ (dex)	E(B-V) (mag)
SDSS J033133.89+010327.9	spSpec-51810-0415-322	35117 (695)	7.885 (0.031)	0.064 (0.031)
SDSS J033133.89+010327.9	spSpec-51879-0415-337	35921 (94)	7.805 (0.013)	0.067 (0.028)
SDSS J033133.89+010327.9	spSpec-52672-0810-389	35358 (635)	7.811 (0.054)	0.084 (0.011)
SDSS J075058.46+491707.3	spSpec-53089-1779-342	24296 (1445)	7.843 (0.058)	0.040 (0.055)
SDSS J075106.52+301726.4	spSpec-52663-0889-621	32973 (308)	7.812 (0.033)	0.000 (0.001)
SDSS J081126.68+053911.9	spSpec-52934-1295-168	27912 (557)	7.808 (0.067)	0.073 (0.073)
SDSS J081234.94+040852.1	spSpec-52641-1184-347	27420 (399)	7.753 (0.044)	0.031 (0.014)
SDSS J082346.15+245345.7	spSpec-52962-1585-605	33892 (212)	7.709 (0.042)	0.011 (0.011)
SDSS J084537.74+065346.2	spSpec-52964-1298-151	22062 (663)	8.410 (0.038)	0.040 (0.055)
SDSS J091558.19+201606.2	spSpec-53699-2288-223	24409 (475)	8.230 (0.064)	0.014 (0.014)
SDSS J091601.87+200758.1	spSpec-53699-2288-194	32102 (401)	7.184 (0.020)	0.027 (0.068)
SDSS J092010.55+045721.1	spSpec-52707-0991-221	62729 (2648)	7.266 (0.097)	0.051 (0.044)
SDSS J094203.19+544630.2	spSpec-51991-0556-112	28746 (388)	7.877 (0.019)	0.000 (0.002)
SDSS J094940.37+032425.5	spSpec-52286-0571-257	49492 (2205)	7.432 (0.129)	0.032 (0.048)
SDSS J095230.44+114202.3	spSpec-53054-1743-184	27294 (330)	7.855 (0.018)	0.004 (0.004)
SDSS J095245.59+020938.9	spSpec-51908-0481-506	44492 (1453)	7.639 (0.047)	0.000 (0.095)
SDSS J100222.50+292755.0	spSpec-53436-1950-124	70874 (5659)	7.372 (0.200)	0.000 (0.095)
SDSS J100543.92+304744.7	spSpec-53358-1953-378	66984 (4732)	7.511 (0.036)	0.001 (0.094)
SDSS J100614.76+441906.3	spSpec-52703-0942-636	55721 (3152)	7.639 (0.147)	0.000 (0.095)
SDSS J101328.17+061207.4	spSpec-52641-0996-066	49416 (2060)	7.740 (0.026)	0.004 (0.091)
SDSS J103743.48+485720.8	spSpec-52354-0875-133	21179 (213)	8.130 (0.017)	0.054 (0.041)
SDSS J103907.38+081840.9	spSpec-52734-1240-097	23564 (402)	7.386 (0.069)	0.050 (0.045)
SDSS J104332.62+445329.0	spSpec-52992-1431-591	50379 (1496)	7.618 (0.049)	0.001 (0.094)
SDSS J104419.01+405553.0	spSpec-53035-1433-405	27852 (229)	7.718 (0.074)	0.003 (0.086)
SDSS J110634.39+073712.2	spSpec-52723-1004-388	36110 (1728)	7.703 (0.093)	0.082 (0.013)
SDSS J114152.63+253533.9	spSpec-53856-2505-581	45697 (3797)	7.556 (0.103)	0.019 (0.076)
SDSS J120525.01+303444.7	spSpec-53729-2225-617	29958 (227)	7.766 (0.046)	0.000 (0.013)
SDSS J121205.11+140801.8	spSpec-53466-1765-136	21154 (316)	8.306 (0.033)	0.019 (0.019)
SDSS J121845.69+264831.8	spSpec-53816-2231-133	26341 (384)	7.790 (0.010)	0.020 (0.045)
SDSS J122336.20+412242.7	spSpec-53112-1452-206	23236 (700)	7.937 (0.034)	0.000 (0.003)
SDSS J124407.67+582351.9	spSpec-52765-1317-405	32179 (143)	7.896 (0.016)	0.000 (0.095)
SDSS J125217.15+154443.2	spSpec-53171-1770-567	26290 (611)	7.239 (0.055)	0.014 (0.016)
SDSS J130234.44+101239.0	spSpec-53883-1793-508	43656 (319)	7.760 (0.071)	0.020 (0.073)
SDSS J132232.12+641545.8	spSpec-52056-0603-477	29074 (89)	7.339 (0.100)	0.000 (0.002)
SDSS J132434.39+072525.3	spSpec-53556-1799-497	27648 (83)	7.851 (0.079)	0.005 (0.005)
SDSS J133207.33+665453.4	spSpec-51989-0497-346	27701 (1373)	7.862 (0.061)	0.000 (0.002)
SDSS J133514.52+505012.3	spSpec-53433-1669-350	38139 (2010)	7.765 (0.173)	0.048 (0.047)
SDSS J134430.11+032423.2	spSpec-52025-0529-572	26187 (101)	7.825 (0.010)	0.028 (0.028)
SDSS J140327.76+002119.6	spSpec-51942-0301-626	65315 (4775)	7.461 (0.198)	0.019 (0.076)
SDSS J142020.80+521549.3	spSpec-52725-1045-609	24548 (480)	7.757 (0.022)	0.055 (0.055)
SDSS J143059.88+100142.9	spSpec-53533-1709-187	24910 (576)	7.824 (0.046)	0.000 (0.032)
SDSS J143105.74+042215.6	spSpec-52027-0585-495	23740 (565)	7.755 (0.093)	0.025 (0.025)
SDSS J143315.92+252853.1	spSpec-53827-2135-156	23860 (290)	7.137 (0.012)	0.010 (0.010)
SDSS J143443.25+533521.2	spSpec-52764-1326-639	22667 (188)	7.755 (0.044)	0.033 (0.033)
SDSS J144814.08+282511.7	spSpec-53764-2141-127	24478 (1657)	8.332 (0.047)	0.000 (0.001)
SDSS J145415.84+551152.3	spSpec-52353-0792-285	28680 (332)	8.285 (0.025)	0.000 (0.002)
SDSS J145600.81+574150.8	spSpec-52056-0610-288	31989 (341)	7.634 (0.050)	0.000 (0.002)
SDSS J150045.01+621107.2	spSpec-52339-0609-039	23452 (481)	7.765 (0.013)	0.000 (0.003)
SDSS J150422.29+621718.6	spSpec-52055-0611-538	63549 (2154)	7.548 (0.221)	0.000 (0.095)
SDSS J151421.26+004752.8	spSpec-51689-0312-371	29080 (121)	7.749 (0.013)	0.046 (0.008)
SDSS J152041.96+495140.8	spSpec-52751-1166-270	29809 (67)	7.333 (0.106)	0.000 (0.095)
SDSS J152839.42+011300.1	spSpec-51641-0314-331	54435 (4570)	7.730 (0.184)	0.090 (0.006)
SDSS J160839.07+074542.5	spSpec-53498-1730-199	23508 (89)	8.464 (0.060)	0.026 (0.026)
SDSS J165318.76+371027.2	spSpec-52433-0820-328	20599 (1109)	8.198 (0.010)	0.000 (0.002)
SDSS J165851.11+341853.3	spSpec-52435-0972-475	58350 (866)	7.635 (0.023)	0.000 (0.095)
SDSS J170331.62+223251.3	spSpec-53462-1688-188	25687 (1629)	7.840 (0.018)	0.076 (0.076)
SDSS J172406.14+562003.1	spSpec-51818-0358-318	36442 (103)	7.267 (0.016)	0.000 (0.095)
SDSS J212412.14+110415.7	spSpec-52466-0730-392	22759 (237)	7.772 (0.078)	0.011 (0.011)
SDSS J214001.05-075052.2	spSpec-52824-1177-480	31605 (402)	7.753 (0.059)	0.027 (0.068)

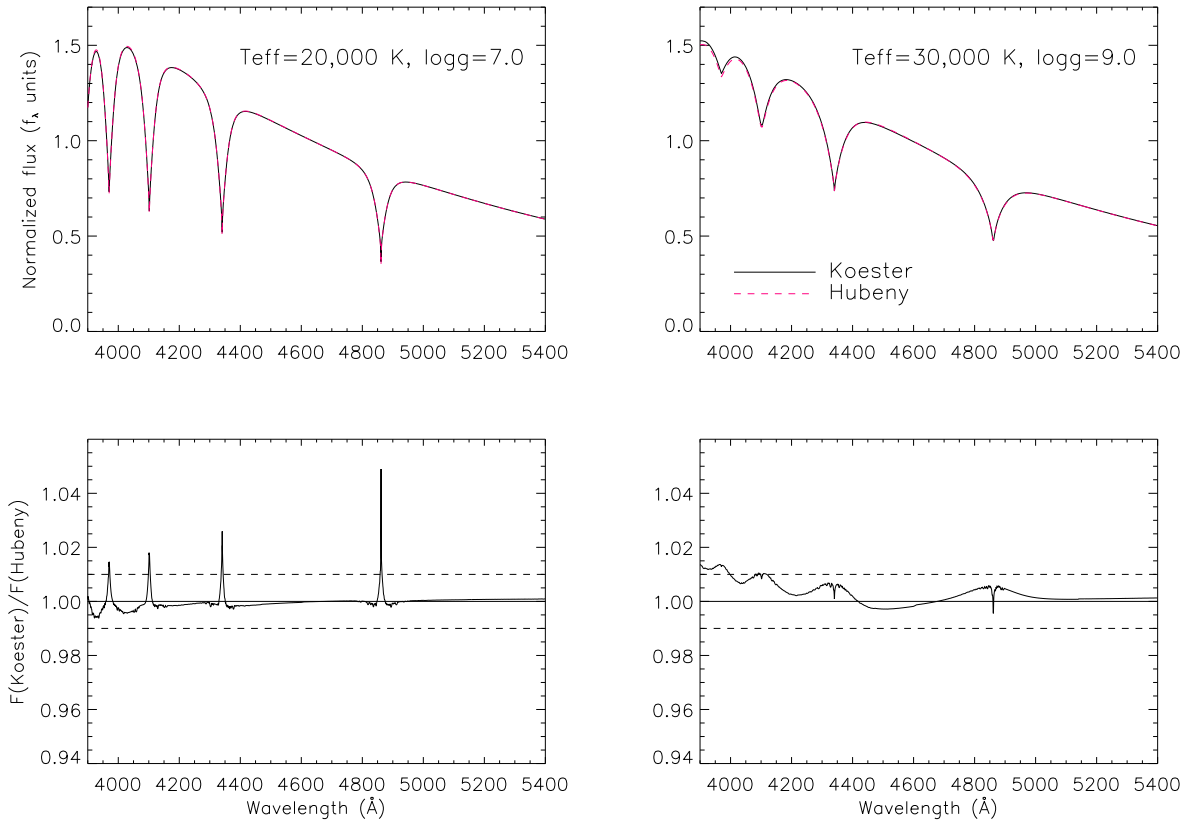

Figure 1. A comparison between the model fluxes for DA white dwarfs predicted from the LTE model atmospheres by Koester (private communication, black line), and Hubeny (red line). Only the shape of the spectrum is of interest for our purposes, and the fluxes are arbitrarily normalized by a constant to match perfectly at $\log\lambda = 3.67$ (4677.352 Å). The lower panels show the flux ratios

0.005 mag, using the prescription of Fitzpatrick (1999) with $R \equiv A_V/E(B-V) = 3.1$.

The optimization is based on the Nelder-Mead method (Nelder & Mead 1965) assisted by Bezier quadratic interpolation in the grid of synthetic fluxes (see, e.g., Auer 2003). Internal uncertainties are estimated, assuming the errors in the fluxes are normally distributed, from the diagonal of the inverse of the curvature matrix.

3 SAMPLE SELECTION

With the goal of identifying solid DA candidates for a network of flux standards, we scanned the SDSS DR6 photometric catalog in search for hot objects satisfying $(u-g)_0 < 0.6$ and $(g-r)_0 < -0.2$. We also imposed the constraint of a moderate estimated extinction towards the sources: $A_g < 0.827$, with A_g from the dust maps of Schlegel, Finkbeiner & Davis (1998). This is approximately equivalent to $E(B-V) < 0.27$ mag, but this value would only apply to objects outside the Milky Way, or at least beyond the extinction layer; we will later restrict our analysis to stars with $E(B-V) < 0.1$. To allow a reliable determination of the stellar parameters, necessary to assign unique theoretical spectral energy distributions, we also limited our search to relatively bright sources ($14 < g < 17$). Our query to the SDSS Catalog Archive Server (CAS; Thakar et al. 2008) returned 598 objects[2].

Viable DA candidates must show spectra that are well matched by DA models. Thus, we downloaded the spectra for all the selected targets and analyzed them following the prescription in §2. The quality of the fittings was assessed from the χ^2 statistics, and used to select the sources that were closely approximated by theoretical fluxes for DA stars. Although white dwarfs are very dim, at the faint magnitudes covered by the SDSS hot DA are at distances of a few hundred pc, and extinction becomes significant, at least when aiming at modeling flux distributions with high accuracy.

The radial velocities determined by the SDSS pipeline were used to correct the Doppler shifts in the spectra before the analysis, and both the model fluxes and the observed spectra were normalized to have a median flux equal to one in the wavelength range used in the analysis. Only 57 objects which spectra were matched by the model fluxes with $\chi^2 < 0.63$ and with derived atmospheric parameters $21,000 < T_{\rm eff} < 85,000$K and $7.1 < \log g < 9.4$, and limited extinction, $0.0 \leqslant E(B-V) < 0.095$, were retained for further analysis. Fig. 2 shows a few representative examples of the fittings in the case where the spectra are normalized

[2] The query returned, in fact, 599 sources, but one file ("spSpec-53388-1937-316.fit") had an anomalous format.

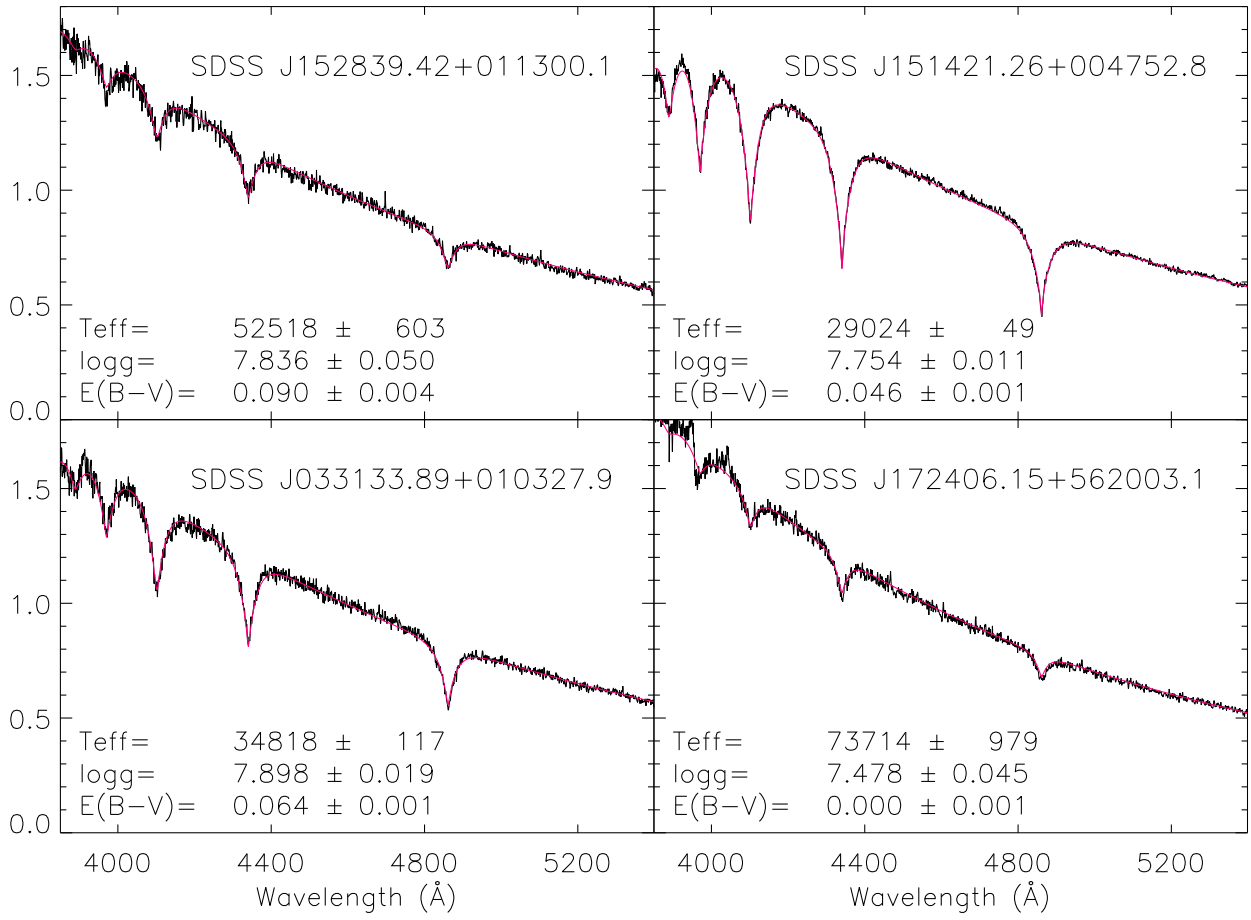

Figure 2. Model fittings to four of the SDSS sample stars. The fluxes are in f_λ units, normalized to have a median of value of one in the range 3850–5400 Å. Note that the parameters here do not match those in Table 1, as the table gives the average results for two types of analyses: those using spectra that preserve continuum information such as those shown here, and those using continuum-corrected spectra.

by their median fluxes in the analysis window. As mentioned earlier, we also analyzed the spectra after rectifying the continuum shape.

In Fig. 3 we show the determined atmospheric parameters for the sample. As expected, the derived gravities decrease smoothly for hotter stars (see, e.g. Althaus et al. 2005). At least in the range $20,000 < T_{\rm eff} < 40,000$ K, three clear groups are apparent. These likely correspond to the three mass clusters found for DA white dwarfs in studies using the Palomar Green survey (Liebert et al. 2005), and in earlier SDSS data releases (e.g. Kepler et al. 2007, DeGennaro et al. 2008). Perhaps due to our strict selection criteria for the quality of the fittings, and the resulting minute error bars, the three groups appear here more cleanly separated than in previous reports. We note that heavy elements are more commonly found in the atmospheres of DA stars hotter than 50,000 K (Barstow et al. 2003b), making such stars statistically more vulnerable to underestimated effective temperatures when their hydrogen lines are interpreted with pure-H model atmospheres (Barstow, Hubeny & Holberg 1998).

Kilic et al. (2007) considered both continuum-corrected fluxes and relative fluxes on the determination of atmospheric parameters for DA white dwarfs from medium resolution MMT spectra. Their conclusion was that using well-calibrated relative fluxes helped considerably to reduce degeneracies, and no significant systematic differences in the inferred surface gravities were apparent. The continuum-corrected spectra are immune to the distortions of interstellar extinction, and therefore similar surface temperatures obtained by the two methods places a limit to the interstellar absorption that the spectra in our sample have suffered.

We repeated such an experiment for the particular case of the SDSS spectra considered in this work. Reddening needs not be considered when analyzing the continuum-corrected spectra. However, if reddening is neglected (forcing $E(B-V) = 0$) in the analysis of spectra containing continuum information, a systematic trend is apparent. This is illustrated in Fig. 4, where the derived $T_{\rm eff}$ from continuum-corrected spectra are typically higher, in particular for the hotter stars, in line with the expected signature of interstellar reddening. When reddening is considered, such trend is effectively removed, and the agreement between the two methods greatly improved, as shown in Fig. 4. Systematic differences are also present in $\log g$, for both cases (with and without reddening corrections), but these are also reduced

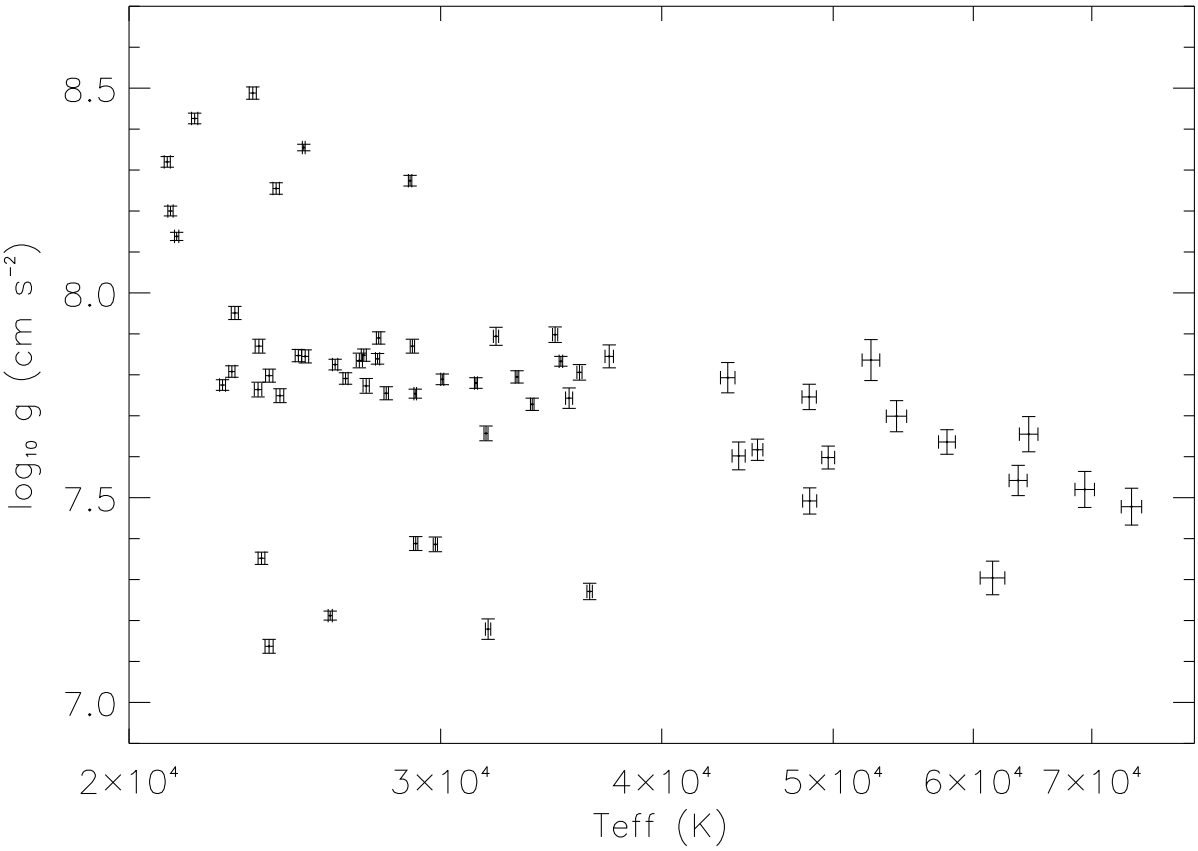

Figure 3. $T_$eff and $\log g$ derived from the analysis of spectra with continuum information such as those illustrated in Fig. 2. The uncertainties are internal and do not consider systematic errors in the models or the observations. Note that a non-linear scale is being used for the abscissae for the sake of clarity.

when reddening is accounted for and have nevertheless a far smaller impact on the absolute fluxes.

The results based on spectra with continuum information are more precise, but are also more exposed to systematic errors in the SDSS flux calibration. Our analysis of such spectra, when reddening is considered, returns parameters that are on the same scale as those from continuum-rectified spectra. Therefore, we adopt as the final parameters ($T_{\rm eff}$ and $\log g$) the weighted average of the two analyses. It is also noticeable in Fig. 4 that the internal random errors derived from each method are not always consistent. Conservatively, we adopt as $1-\sigma$ uncertainties the sum in quadrature of the estimated random uncertainties and the systematic difference between the two methods. By fitting the spectra with continuum information with the $T_{\rm eff}$ and $\log g$ fixed to the average values and allowing $E(B-V)$ to vary, we derive an estimate for the uncertainty in $E(B-V)$ for each star, which is again added in quadrature with the internal uncertainty to obtain the final estimate. The final adopted parameters are given in Table 1. Typical (median values) uncertainties are 1.8 %, 0.047 dex, and 0.032 mag in $T_{\rm eff}$, $\log g$, and $E(B-V)$, respectively. These uncertainties in $T_{\rm eff}$ and $\log g$ are slightly larger than those inferred by Liebert et al. (2005) for their analysis of spectra with typically higher signal-to-noise ratios but lower resolution. There are three spectra of the star SDSS J033133.89+010327.9, and the derived parameters are fairly consistent.

Most of the stars in our sample (exactly 43; see Table 1), are included in the SDSS-DR4 catalog of DA stars of Eisenstein et al. (2006). Between 20,000 and 30,000 K, the $T_{\rm eff}$ values of Eisenstein et al. are lower than ours by a few percent, and the trend reverses for warmer temperatures, with the Eisenstein et al. values being up to ~ 10 % higher than ours at about 65,000 K. We find good agreement between our surface gravities and those from the SDSS-DR4 catalog at the lowest temperatures in our sample ($\sim 20,000$ K), but growing discrepancies at warmer temperatures, with the SDSS-DR4 values being ~ 0.25 dex higher around 65,000 K. There are 15 stars included in Table 1 which are also part in the catalog of DA stars from the Palomar Green survey (Liebert et al. 2005). The Liebert et al. surface temperatures are also a few percent lower than ours in the range $20,000 < T_{\rm eff} < 20,000$ K, but they are lower by as much as 10 % at about 60,000 K. Their surface gravities are systematically higher by 0.08 ± 0.02 dex, and it should be noted that a similar discrepancy was also found by Liebert et al. when they compared their gravities with several other investigations (Finley et al. 1997, Marsh et al. 1997, Homeier et

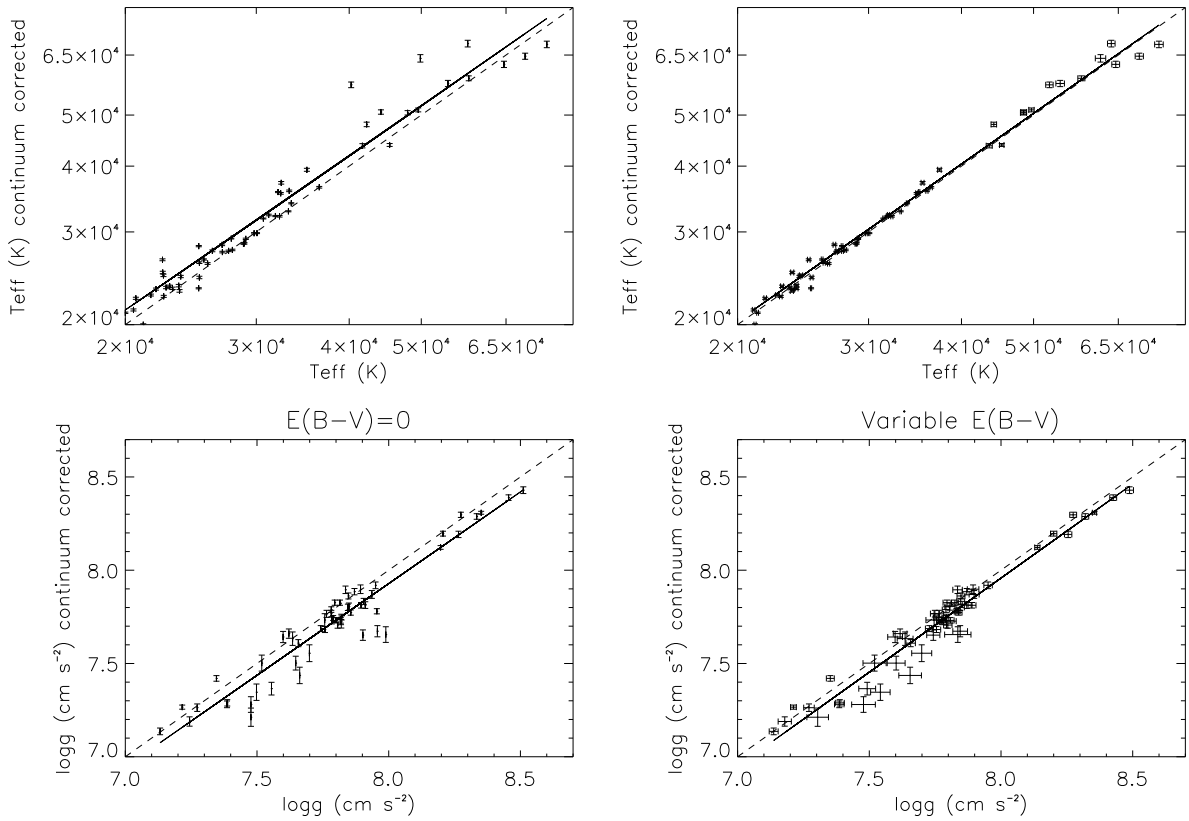

Figure 4. Comparison between the atmospheric parameters retrieved for our SDSS sample stars using continuum-corrected spectra and spectra that preserve the continuum shape. The left-hand panels correspond to the case when reddening is neglected, while the right-hand panels correspond to an analysis that accounts for reddening

al. 1998, Koester et al. 2001). In the hot end, our temperature scale is intermediate between those of Eisenstein et al. and Liebert et al., which differ from each other by ~ 20 %.

4 ABSOLUTE FLUXES

Once the atmospheric parameters, surface gravity and effective temperature, have been determined for the DA, their surface radiative flux is given by the corresponding model atmospheres. Only a small part of their spectrum ($385-540$ nm) is actually used in the parameter determination described above, but the employed grid of model fluxes extends to the entire optical region ($300-700$ nm), and therefore we determine absolute fluxes for the broader spectral region.

The quantity of interest is the flux received at the Earth, which is related to the stellar surface flux provided by the model atmosphere by the angular diameter, or more precisely by the square of the ratio of the distance between the star and the Earth and the stellar radius. Fairly accurate estimates for the radii of DA white dwarfs are possible based on models, but no direct estimates are available for the distances to these faint DA. A direct approach that can be followed instead is to use broad-band photometry to scale the theoretical flux distributions. Fig. 5 illustrates the span of the SDSS *ugr* bands and the coverage of the theoretical spectra. With a typical uncertainty of 0.02 mag in each filter, considering the three together gives an expected uncertainty in the absolute scale of the fluxes of about 1%. This figure is comparable or smaller than the expected uncertainty in the relative fluxes, but it presumes no systematics.

In practice, we derive synthetic absolute fluxes at the stellar surface for the corresponding atmospheric parameters and extinction for each DA by interpolation in our grid, and determine synthetic photometry in the *ugr* bands using the filter responses for point sources observed at an airmass of 1.3 available from the SDSS web pages[3]. For clarity, we refer to the observed magnitudes with letters in italic (*ugr*, indicating SDSS PSF magnitudes as extracted from the DR6 CAS) and to those calculated at the stellar surface in bold (**ugr**). For each star, the difference between the magnitudes computed for the the photosphere and those measured at the Earth can be derived for each band as $\delta m \equiv m - \mathbf{m}$, with $m(\mathbf{m})$ replaced by u, g or r (**u**, **g** or **r**). In the absence of systematic errors, these three values will be consistent and

$$\delta m \equiv m - \mathbf{m} = -2.5 \log \left(\frac{R}{d} \right)^2 , \qquad (1)$$

where R is the stellar radius, and d the distance to the star. (Recall that the effect of interstellar extinction is already included in the model magnitudes m).

[3] http://www.sdss.org/dr3/instruments/imager/index.html#filters

Table 2. SDSS Photometry and zero points.

Name	u	g	r	δu	δg	δr	δ (g and r)
SDSS J033133.89+010327.9	16.183 (0.022)	16.432 (0.013)	16.876 (0.012)	56.633	56.587	56.632	56.610 (0.023)
SDSS J033133.89+010327.9	16.183 (0.022)	16.432 (0.013)	16.876 (0.012)	56.717	56.651	56.675	56.663 (0.012)
SDSS J033133.89+010327.9	16.183 (0.022)	16.432 (0.013)	16.876 (0.012)	56.747	56.678	56.701	56.689 (0.012)
SDSS J075058.46+491707.3	16.664 (0.015)	16.740 (0.018)	17.117 (0.018)	56.294	56.263	56.267	56.265 (0.002)
SDSS J075106.52+301726.4	15.649 (0.015)	15.917 (0.020)	16.310 (0.022)	56.351	56.265	56.169	56.217 (0.048)
SDSS J081126.68+053911.9	16.261 (0.016)	16.416 (0.012)	16.778 (0.010)	56.126	56.110	56.103	56.107 (0.004)
SDSS J081234.94+040852.1	16.723 (0.016)	16.860 (0.012)	17.302 (0.009)	56.737	56.674	56.700	56.687 (0.013)
SDSS J082346.15+245345.7	15.273 (0.028)	15.552 (0.025)	16.039 (0.014)	55.984	55.911	55.916	55.914 (0.003)
SDSS J084537.74+065346.2	16.539 (0.018)	16.637 (0.016)	16.972 (0.014)	55.932	55.967	55.968	55.968 (0.001)
SDSS J091558.19+201606.2	16.529 (0.013)	16.590 (0.015)	17.026 (0.010)	56.316	56.221	56.261	56.241 (0.020)
SDSS J091601.87+200758.1	16.674 (0.013)	16.941 (0.015)	17.395 (0.010)	57.160	57.130	57.123	57.126 (0.003)
SDSS J092010.55+045721.1	16.274 (0.019)	16.673 (0.016)	17.188 (0.010)	57.652	57.624	57.659	57.642 (0.017)
SDSS J094203.19+544630.2	16.714 (0.013)	16.934 (0.017)	17.398 (0.016)	57.027	56.975	56.977	56.976 (0.001)
SDSS J094940.37+032425.5	16.454 (0.020)	16.787 (0.016)	17.301 (0.014)	57.656	57.571	57.595	57.583 (0.012)
SDSS J095230.44+114202.3	16.317 (0.022)	16.472 (0.016)	16.869 (0.019)	56.454	56.379	56.331	56.355 (0.024)
SDSS J095245.59+020938.9	16.026 (0.015)	16.347 (0.021)	16.832 (0.018)	57.250	57.135	57.099	57.117 (0.018)
SDSS J100222.50+292755.0	15.677 (0.010)	16.136 (0.011)	16.669 (0.016)	57.428	57.395	57.382	57.388 (0.007)
SDSS J100543.92+304744.7	15.967 (0.023)	16.346 (0.018)	16.904 (0.013)	57.651	57.544	57.558	57.551 (0.007)
SDSS J100614.76+441906.3	16.401 (0.024)	16.824 (0.014)	17.369 (0.014)	57.892	57.846	57.856	57.851 (0.005)
SDSS J101328.17+061207.4	15.845 (0.018)	16.280 (0.019)	16.754 (0.021)	57.180	57.165	57.116	57.141 (0.024)
SDSS J103743.48+485720.8	15.275 (0.021)	15.303 (0.021)	15.648 (0.015)	54.475	54.501	54.533	54.517 (0.016)
SDSS J103907.38+081840.9	16.222 (0.007)	16.180 (0.017)	16.595 (0.021)	55.701	55.604	55.656	55.630 (0.026)
SDSS J104332.62+445329.0	16.271 (0.012)	16.673 (0.014)	17.183 (0.016)	57.644	57.591	57.573	57.582 (0.009)
SDSS J104419.01+405553.0	16.660 (0.028)	16.832 (0.040)	17.237 (0.017)	56.855	56.788	56.739	56.763 (0.024)
SDSS J110634.39+073712.2	16.548 (0.011)	16.878 (0.030)	17.305 (0.025)	57.047	57.076	57.098	57.087 (0.011)
SDSS J114152.63+253533.9	16.620 (0.026)	16.990 (0.029)	17.480 (0.016)	57.787	57.736	57.725	57.731 (0.005)
SDSS J120525.01+303444.7	15.697 (0.024)	15.877 (0.022)	16.300 (0.014)	56.132	56.016	55.965	55.990 (0.026)
SDSS J121205.11+140801.8	16.810 (0.012)	16.811 (0.020)	17.153 (0.014)	56.186	56.139	56.132	56.136 (0.003)
SDSS J121845.69+264831.8	16.320 (0.011)	16.469 (0.012)	16.861 (0.021)	56.272	56.237	56.211	56.224 (0.013)
SDSS J122336.20+412242.7	16.887 (0.019)	16.926 (0.026)	17.285 (0.020)	56.593	56.512	56.465	56.488 (0.024)
SDSS J124407.67+582351.9	16.589 (0.017)	16.846 (0.026)	17.300 (0.018)	57.231	57.144	57.114	57.129 (0.015)
SDSS J125217.15+154443.2	14.339 (0.033)	14.403 (0.029)	14.800 (0.021)	54.294	54.189	54.150	54.169 (0.020)
SDSS J130234.44+101239.0	16.627 (0.018)	16.988 (0.018)	17.470 (0.024)	57.729	57.677	57.663	57.670 (0.007)
SDSS J132232.12+641545.8	16.054 (0.017)	16.268 (0.024)	16.658 (0.016)	56.381	56.333	56.249	56.291 (0.042)
SDSS J132434.39+072525.3	16.417 (0.019)	16.581 (0.018)	17.006 (0.023)	56.586	56.513	56.491	56.502 (0.011)
SDSS J133207.33+665453.4	16.669 (0.017)	16.812 (0.026)	17.342 (0.015)	56.869	56.767	56.844	56.806 (0.039)
SDSS J133514.52+505012.3	16.484 (0.017)	16.781 (0.013)	17.262 (0.013)	57.247	57.190	57.221	57.205 (0.016)
SDSS J134430.11+032423.2	16.482 (0.015)	16.603 (0.018)	17.005 (0.016)	56.380	56.328	56.323	56.326 (0.002)
SDSS J140327.76+002119.6	16.410 (0.022)	16.856 (0.017)	17.376 (0.018)	57.981	57.962	57.963	57.963 (0.000)
SDSS J142020.80+521549.3	16.753 (0.024)	16.855 (0.018)	17.273 (0.015)	56.334	56.342	56.401	56.371 (0.030)
SDSS J143059.88+100142.9	16.537 (0.022)	16.629 (0.019)	17.044 (0.017)	56.428	56.355	56.343	56.349 (0.006)
SDSS J143105.74+042215.6	16.808 (0.014)	16.791 (0.020)	17.174 (0.011)	56.443	56.325	56.321	56.323 (0.002)
SDSS J143315.92+252853.1	16.810 (0.030)	16.772 (0.021)	17.168 (0.015)	56.509	56.373	56.351	56.362 (0.011)
SDSS J143443.25+533521.2	15.921 (0.017)	15.942 (0.021)	16.248 (0.012)	55.390	55.354	55.294	55.324 (0.030)
SDSS J144814.08+282511.7	14.254 (0.025)	14.398 (0.023)	14.802 (0.014)	54.121	54.088	54.081	54.085 (0.003)
SDSS J145415.84+551152.3	15.584 (0.013)	15.813 (0.014)	16.275 (0.016)	55.908	55.851	55.859	55.855 (0.004)
SDSS J145600.81+574150.8	15.951 (0.022)	16.191 (0.020)	16.679 (0.016)	56.569	56.475	56.476	56.476 (0.000)
SDSS J150045.01+621107.2	16.909 (0.016)	16.961 (0.020)	17.326 (0.020)	56.632	56.565	56.518	56.541 (0.024)
SDSS J150422.29+621718.6	16.328 (0.017)	16.808 (0.018)	17.277 (0.018)	57.962	57.958	57.886	57.922 (0.036)
SDSS J151421.26+004752.8	15.483 (0.012)	15.687 (0.012)	16.103 (0.012)	55.603	55.579	55.583	55.581 (0.002)
SDSS J152041.96+495140.8	16.037 (0.040)	16.268 (0.026)	16.722 (0.034)	56.442	56.392	56.368	56.380 (0.012)
SDSS J152839.42+011300.1	16.168 (0.016)	16.547 (0.019)	17.037 (0.014)	57.195	57.200	57.266	57.233 (0.033)
SDSS J160839.07+074542.5	16.653 (0.019)	16.690 (0.016)	17.093 (0.016)	56.290	56.199	56.236	56.218 (0.019)
SDSS J165318.76+371027.2	16.563 (0.019)	16.498 (0.012)	16.843 (0.013)	55.954	55.847	55.826	55.837 (0.011)
SDSS J165851.11+341853.3	15.774 (0.011)	16.173 (0.015)	16.697 (0.012)	57.315	57.240	57.227	57.234 (0.007)
SDSS J170331.62+223251.3	16.496 (0.016)	16.608 (0.011)	17.002 (0.013)	56.106	56.109	56.158	56.134 (0.025)
SDSS J172406.14+562003.1	15.830 (0.021)	16.029 (0.022)	16.419 (0.014)	56.741	56.557	56.438	56.497 (0.059)
SDSS J212412.14+110415.7	16.835 (0.022)	16.792 (0.013)	17.165 (0.012)	56.424	56.295	56.276	56.286 (0.010)
SDSS J214001.05-075052.2	15.756 (0.020)	16.019 (0.012)	16.460 (0.013)	56.212	56.174	56.164	56.169 (0.005)

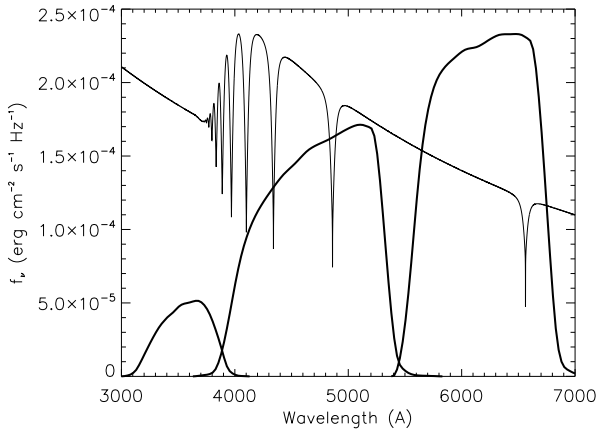

Figure 5. Model flux for a DA white dwarf with $T_{\rm eff} = 20,000$ and $\log g = 7.0$. The shapes of the SDSS photometric passbands (ugr) are shown with thick lines, arbitrarily scaled.

Table 3 gives the observed magnitudes and the δ values for each star. There is an average offset $< \delta u - \delta g >= 0.0590 \pm 0.0056$ mag, but the results are more consistent for g and r with $< \delta r - \delta g >= -0.0068 \pm 0.0051$ mag. The observed u magnitudes should be reduced by 0.04 magnitudes to place them on the AB system (Oke & Gunn 1983), as recommended in the SDSS web pages (www.sdss.org; see also the discussions in Eisenstein et al. 2006, Ivezić et al. 2007). However, after applying this correction, the values for δu we derive are still offset from those for g and r by 0.02 mag. There is no dramatic variation in the uncertainties in the observations for each filter, with median values of 0.0179, 0.0176, and 0.0150 mag for u, g, and r, respectively, but dropping u seems the most sensible option. There are known issues with the u filters, such as flatfielding problems, a red leak which might affect the observations particularly if there are nearby unresolved cooler objects (Adelman-McCarthy et al. 2008, Stoughton et al. 2002), and a recently discovered variation with time of the effective filter transmission caused, most likely, by a degradation of the UV coating of the u-band CCDs (Abazajian et al. 2009). In addition, even if the detected $\delta u - \delta g$ offset is removed, the median 1σ scatter in the average δ is 0.025 mag, but this value is reduced to 0.016 mag when only g and r are considered.

5 THE PROPOSED STANDARDS

As discussed in the introduction, the uncertainties in the relative shape of the spectral fluxes computed for DA stars are at the level of < 1 %, but given that we do not know exactly the atmospheric parameters and the amount of interstellar reddening, additional contributions to the error budget need to be considered.

To evaluate the impact of the uncertainties in the derived $T_{\rm eff}$, $\log g$ and $E(B-V)$ on the optical spectral energy distributions assigned to each of the DA, we interpolate fluxes after perturbing each parameter by the expected $1-\sigma$ uncertainty. Because we are normalizing the fluxes of our sample stars to match the SDSS g magnitudes, we normalize the spectra at the weighted average wavelength for the g passband, which is 4686 Å. Fig. 6 illustrates the results for the four stars included in Fig. 2. Depending on the star, the uncertainties in $T_{\rm eff}$ or $E(B-V)$ dominate the errors in the relative fluxes; $\log g$ has always a minor effect. Large errors are observed in the cores of the Balmer lines, which are particularly sensitive to changes in $T_{\rm eff}$ and surface gravity. We combine the three contributions in quadrature to estimate the final uncertainties. Although it is possible to determine and use the internal covariances among the errors in the parameters to estimate the uncertainties in the fluxes, the fact is that the errors in the parameters are dominated by the contributions from the systematic offsets between the analyses using continuum-corrected spectra and those in which the continuum shape is preserved, and therefore we simply assume that the errors are weakly correlated.

The error budget for each of the DA in our sample combines the wavelength-dependent uncertainties in the relative fluxes, just discussed, with those in the zero point magnitudes –set by the average between the observed and predicted fluxes in the g and r bands. Useful flux standards should have reasonable uncertainties. We select only DA stars with an total uncertainty $< 5\%$ at all wavelengths in the optical, and $< 3\%$ between $4500 < \lambda < 7000$ Å. There are 9 stars in our sample that satisfy these criteria. These are compiled in Table 5, where we also provide uncertainty estimates at four different wavelengths. We include the expected errors in the theoretical spectral energy distributions (1 %). The theoretical spectral fluxes at the Earth for these stars are given in electronic format[4].

6 THE HST STANDARDS

As a result of the analysis presented in the previous sections, we have identified a number of stars for which the absolute fluxes have an expected uncertainty < 2 % throughout the optical (see Table 3). An obvious question is how these fare in comparison with the HST standards. To answer this question we follow exactly the same steps as for the SDSS stars: fitting the STIS spectra normalized to their median in the spectral window, or normalized to the continuum, adopting averaged $T_{\rm eff}/\log g$, etc. The original spectra, obtained

[4] These are available from `http://hebe.as.utexas.edu/std/`

Table 3. Proposed spectrophotometric standards and expected fractional errors in their fluxes.

Name	g	$\sigma_{\lambda=3500}$	$\sigma_{\lambda=4500}$	$\sigma_{\lambda=5500}$	$\sigma_{\lambda=6500}$
SDSS J082346.15+245345.7	15.552	0.016	0.011	0.013	0.018
SDSS J094203.19+544630.2	16.934	0.015	0.010	0.010	0.010
SDSS J095230.44+114202.3	16.472	0.028	0.026	0.026	0.027
SDSS J132434.39+072525.3	16.581	0.016	0.015	0.015	0.016
SDSS J143315.92+252853.1	16.772	0.020	0.015	0.016	0.020
SDSS J145415.84+551152.3	15.813	0.014	0.011	0.011	0.011
SDSS J145600.81+574150.8	16.191	0.012	0.010	0.010	0.010
SDSS J151421.26+004752.8	15.687	0.013	0.010	0.012	0.014
SDSS J212412.14+110415.7	16.792	0.020	0.014	0.016	0.020

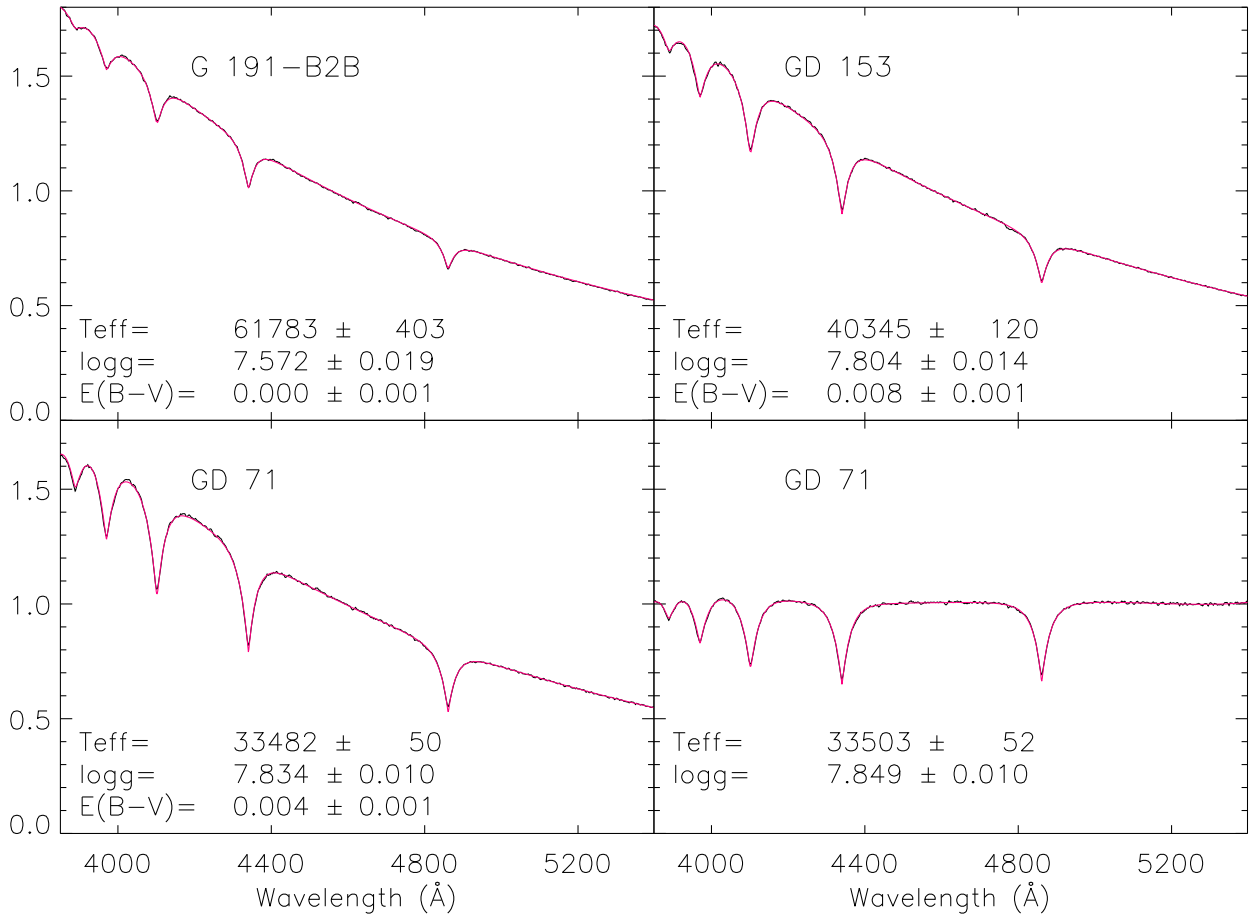

Figure 7. Model fittings to the three HST primary standards. The fluxes are in f_λ units, normalized to have a median value of one in the range 3850–5400 Åin the top and lower-left panels. The lower-right panel illustrates the model fittings for GD 71 in the case when the continuum shape is rectified. Note that the parameters here do not match those in Table 6, as the table gives the average results for two types of analyses: those using spectra that preserve continuum information such as those illustrated in the top and the lower-left panels, and those using continuum-corrected spectra such as the example for GD 71 in the lower-right panel. The use of pure-H models for G 191-B2B is inappropriate as a number of heavy metals have been detected in the UV spectrum of this star.

from the CALSPEC web site, have a resolving power about 1000 in our range of interest (STIS L-mode observations), which is half of the resolution of the SDSS spectra considered earlier, and this taken into account in the analysis. We first assumed that the spectra were at rest, and after finding the best-fitting models, we determined Doppler shifts of +5, −18, and 13 ± 2 km s^{-1} by cross-correlation, corrected them, and repeated the optimizations. We refer the reader to Bohlin, Dickinson & Calzetti (2001, and references therein) for more details about the observations. The derived parameters are given in Table 4. Fig. 7 is the equivalent of Fig. 2 for the HST standards, and includes the fitting to the continuum-rectified spectrum of GD 71. Note that the parameters previously used for assigning model fluxes to these stars were based on LTE model atmospheres.

As a reference, we passed the HST fluxes for the three

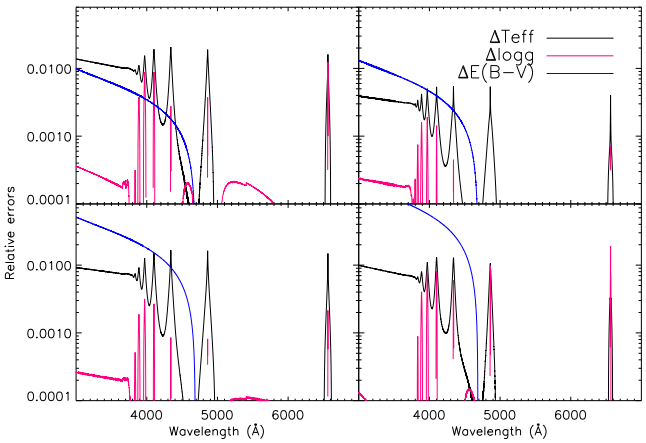

Figure 6. Estimated fractional errors in the relative fluxes for the four stars in Fig. 2.

Table 4. Atmospheric parameters for the three HST standards.

Name	$T_{\rm eff}$ (K)	$\log g$ (dex)	E(B-V) (mag)
G 191 B2B	61980 (514)	7.555 (0.042)	0.000 (0.001)
GD 153	40401 (142)	7.812 (0.018)	0.008 (0.001)
GD 71	33492 (41)	7.841 (0.017)	0.004 (0.001)

standards through the SDSS filter responses for *ugr*. The results are included in Table 5. Holberg & Bergeron performed the same exercise and our results agree with theirs to within 0.003 mag, with the exception of the g band for GD 71, which they found 0.012 mag brighter. As can be seen in the table, the agreement between the derived δm values across the three bands is better than 0.001 mag for G 191 B2B and GD 71, and only slightly larger (0.005 mag) for GD 153, indicating that the good agreement illustrated in Fig. 7 extends to the u and r bands.

To set the zero point of the fluxes we examine first the *ugr* photometry obtained with the Apache Point 0.5-m photometric telescope (PT) and transformed to the 2.5-m SDSS scale (obtained by S. Kent and D. Tucker; published by Holberg & Bergeron 2006). The results are included in Table 6. We note, as Holberg & Bergeron did, an anomalous g-band magnitude for GD 153. After reducing the u magnitudes by 0.04 mag to place them in the AB system, the zero points for G1912B2 and GD 71 agree among the three bands *ugr* to about 0.005 mag. The zero point in GD 153 agrees to 0.001 mag between the u and r bands (again, after reducing u by 0.04 mag), but these disagree with that from the g band by 0.05 mag. Comparing the differences between the synthetic photometry and the observed magnitudes, the δ values, with those determined for the HST spectra, we find an excellent agreement for G 191 B2B and GD 153 (ignoring the g band for the latter). There is, however, a systematic offset of about 0.02 mag between the HST absolute fluxes for GD 71 and the PT photometry for this star.

Given these issues, we consider new photometry obtained using the USNO 1-m telescope. The new observations are described in the Appendix, and the mean *ugr* magnitudes, in the SDSS 2.5-m system, are summarized in Table 5. We prefer the new photometry and will adopt it in the discussion below. The formal uncertainties for the USNO photometry (σ/N; as given in Table 5) are typically smaller than for the PT photometry[5], due to a larger number of measurements available. In addition, while two transformations are required to place the PT photometry on the SDSS 2.5-m *ugriz* system, only one transformation is necessary for the USNO $u'g'r'i'z'$ magnitudes (Tucker et al. 2006). Overall, the scatter between the g and r band scaling factors (δ) is increased relative to the earlier PT photometry, but more in line with expectations at about 1 % (Smith et al. 2002). The newer observations bring the g-band magnitude of GD 153 in line with the scaling factors determined for u and r. More importantly, the 2 % offset between the GD 71 HST fluxes (i.e. the Johnson V magnitude) and the PT photometry is now reduced to less then 1%, and therefore within the expected variance.

For the new USNO photometry we find average offsets $< \delta u - \delta g >= 0.0442 \pm 0.0017$ mag and $< \delta r - \delta g >= +0.0189 \pm 0.0025$ mag. Both of these differ by +0.02 mag from the offsets we determined in §4 for the SDSS DA stars. Because those in §4 correspond to measurements made with the 2.5-m telescope, we consider them more appropriate for the true SDSS system.

The uncertainties in the relative fluxes of these stars due to the uncertainties in their atmospheric parameters and reddening are smaller than the typical values for the SDSS DA stars. This is the result of a much higher signal-to-noise ratio of the STIS spectra, and the fact that the HST standards are brighter and therefore located closer to the Sun and affected by essentially no reddening. Nonetheless, four of the stars in Table 5 have similar uncertainties as the HST standards (SDSS J151421.26+004752.8, SDSS J094203.19+544630.2 and SDSS J145600.81+574150.8). The uncertainties in the absolute fluxes of these stars are dominated by the theoretical errors, which limit their accuracy at about 1%.

Our inferred surface gravities for the three DA standards are in good agreement with the values reported by Barstow et al. (2001, 2003a) from the analysis of Lyman and Balmer line profiles, while our effective temperatures for GD 71 and GD 153 are a few percent higher than those derived in that work. Our temperature for G 191 B2B, however, is about 15 % higher than those given by Barstow et al. from the analysis of Balmer lines, which range between 51500 and 54500 K[6]. The difference between our analysis and the Balmer-based temperatures compiled by Barstow et al. can be attributed to the presence of heavy metals in the atmosphere of this star (see, e.g. Lanz et al. 1999). Our use of a pure-H model leads to an overestimated effective temperature (Barstow, Hubeny & Holberg 1998) by about 6000 K. No metals have been detected in the UV spectrum of GD 153 (Barstow et al. 2003b), but we have not found a similar study including GD 71.

[5] Unlike Holberg & Bergeron (2006), we quote standard errors of the mean in our table, computed from the original table kindly provided by D. Tucker.

[6] We note that the Barstow et al. (2003a) analysis of FUSE spectra for G 191-B2B leads to higher temperatures (about 57000–59000 K), but the differences are believed to be related to difficulties modeling the Lyman series.

Table 5. Photometry and zero points for the three HST standards. The uncertainties quoted correspond to the standard error of the mean from the multiple observations available. The PT photometry includes 7 measurements for G 191-B2B, 1 for GD 153, and 5 in u and 6 in g and r for GD 71. The more recent USNO photometry includes 8 measurements in u and 9 in g and r for G 191-B2B, 4 in all bands for GD 153, and 12 in u and r, and 11 in g for GD 71.

Name	u	g	r	δu	δg	δr	δ (g and r)
			HST spectra				
G 191 B2B	10.990	11.467	12.008	52.597	52.594	52.595	52.594 (<0.001)
GD 153	12.661	13.065	13.578	53.711	53.704	53.713	53.709 (0.005)
GD 71	12.422	12.772	13.259	53.143	53.135	53.136	53.136 (<0.001)
			PT photometry (see Holberg & Bergeron 2006)				
G 191 B2B	11.033 (0.006)	11.470 (0.002)	12.007 (0.003)	52.639	52.597	52.593	52.595 (0.002)
GD 153	12.700	13.022	13.573	53.750	53.661	53.709	53.685 (0.024)
GD 71	12.438 (0.008)	12.752 (0.005)	13.241 (0.005)	53.159	53.115	53.117	53.116 (0.001)
			USNO 1-m photometry (see Appendix)				
G 191-B2B	11.018 (0.004)	11.457 (0.002)	12.013 (0.003)	52.625	52.584	52.600	52.592 (0.008)
GD 153	12.700 (0.002)	13.064 (0.002)	13.592 (0.001)	53.750	53.704	53.727	53.715 (0.012)
GD 71	12.442 (0.004)	12.755 (0.003)	13.259 (0.002)	53.163	53.118	53.136	53.127 (0.009)

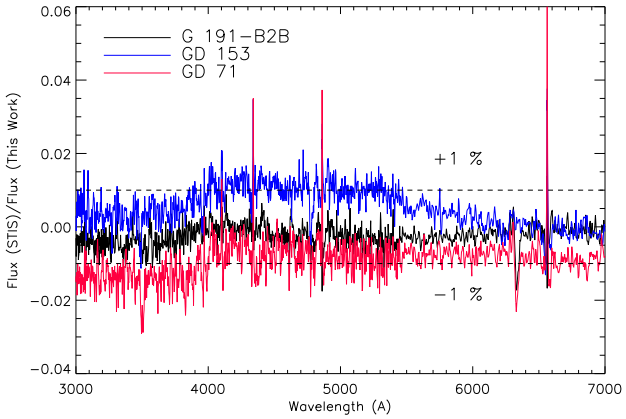

Figure 8. Ratio between the CALSPEC fluxes and those calculated here using redetermined atmospheric parameters for the HST primary standards. The zero point of the flux scale of the CALSPEC fluxes is given by Landolt V-band photometry, while here it is set by SDSS PT ugr photometry (but see text for an exception for GD 153). The two scales are inconsistent by 1.5 % for GD 71.

In Fig. 8 we confront our absolute fluxes for the these stars with those in the CALSPEC library. There is good agreement between the spectral shapes, with the differences caused mainly by the different effective temperatures used to these stars by Bohlin (2000; traceable to Finley, Koester & Basri 1997) – our values are higher by 1, 4 and 2 % for G 191-B2B, GD 153 ad GD 71, respectively. As explained above, our inferred effective temperature for G191-B2B is overestimated by about 6000 K, but it is close to that adopted for calibration of the HST fluxes of this star, and hence the *apparent* good agreement shown in Fig. 8. The consistency between the HST and our fluxes is best in the red, but overall, the discrepancies are limited to < 1.5 %, in line with our expectations.

Close inspection of the residuals in Fig. 8, ignoring G 191-B2B, suggests that there is a systematic offset between the u (3000–4000 Å) and g-band (4000–5500 Å) fluxes. The HST fluxes in the u band are lower than those presented here by about 1 %. The most likely explanation for this feature is the fact that the effective temperatures adopted in the HST calibration for these stars are lower by 2–4 %.

7 CONCLUSIONS

In this paper we consider the possibility of building an extended network of spectrophotometric standard stars by identifying well-behaved pure-hydrogen white dwarfs, spectroscopically determining their atmospheric parameters and reddening, and assigning them absolute fluxes based on model atmosphere calculations scaled with broad-band photometric observations. This procedure was successfully used for defining the three primary flux standards for the HST (Finley, Basri & Bowyer 1990; Bohlin, Colina & Finley 1995; Bohlin 2000), and could be now applied more extensively to many other DA stars that are being identified in ongoing and planned spectroscopic surveys.

We put this idea to work using publicly available spectra from the Sloan Digital Sky Survey. We identify 59 spectra of 57 stars that are nicely reproduced by NLTE DA models, and measured their atmospheric parameters. By comparing the effective temperatures derived from spectra that have been continuum rectified and those which preserve the overall spectral shape we see the effects of reddening in the hotter (and therefore more distant) stars. By including reddening in the analysis the two sets of temperatures are brought into agreement.

Our exercise identifies a set of nine new standard candidates with estimated flux uncertainties less than 3% between 4500 and 7000 Å. We present these stars as *potentially* useful standard sources. Their observed spectral energy distributions are nicely matched with DA white dwarf

models across the visible, and although we have not verified that their fluxes are stable, all the sources are significantly warmer than the ZZ Ceti window ($\sim 11,000$ K), and therefore it is unlikely that they show measurable pulsations. Nevertheless, we should exercise caution if trying to use them as standards at shorter or, especially, longer wavelengths. Some of these stars could have low-mass stellar or sub-stellar companions which could make their fluxes at longer wavelengths to deviate from the predictions from the stellar models. There could also be unresolved nearby objects with variable fluxes whose presence went unnoticed in the observations analyzed here.

From the comparison of the scaling factors between synthetic and observed photometry for the full DA sample we find the following offsets: $< \delta u - \delta g >= 0.059 \pm 0.006$ mag and $< \delta g - \delta r >= -0.007 \pm 0.005$ mag. Assuming the g and the r-bands correspond exactly to AB magnitudes (see, e.g., the discussion by Eisenstein et al. 2006), and that the pure-H models provide accurate descriptions of the spectral energy distribution of the DA stars, the derived $\delta u - \delta g$ difference could simply correspond to the AB mag correction for the u band. However, we note that Holberg & Bergeron (2006) found indication of an offset of -0.02 mag between the SDSS magnitudes for 107 DA white dwarfs in the g band and their fluxes in the Johnson V band.

We carry out a reanalysis of the STIS spectra for the three primary HST standards GD 71, GD 153 and G 191-B2B. We use NLTE model atmospheres to determine their atmospheric parameters, and find effective temperatures that are hotter by 1–4 % compared to those adopted based on an LTE analysis. Our predicted fluxes for the three standards, scaled using *ugriz* photometry, agree at a 1 % level with the adopted HST fluxes.

Heavy metals are present in the atmosphere of G 191-B2B, and our analysis based on pure-H models results in an effective temperature overestimated by about 6000 K. The good agreement for GD 153 and GD 71 demonstrates consistency, but that found for G 191-B2B is simply an artifact and highlights that the spectral energy distribution adopted for this standard needs to be revised. Our analysis also unveils an inconsistency between the photometry obtained for GD 71 with the Apache Point 0.5-m Photometric Telescope, and the zero point of the STIS fluxes for this star, which is based on Landolt (1992) V-band photometry, but the discrepancy is greatly reduced when considering new $u'g'r'$ photometry from the USNO 1-m telescope. Overall, our study supports the level of accuracy presumed for the HST standards, but we also find room for improvement at the 1 % level.

ACKNOWLEDGMENTS

We are thankful to Douglas Tucker for comments about the uncertainties of the PT photometry, and to Ralph Bohlin for useful discussions about HST spectrophotometry. Jay Holberg provided a number of stimulating comments which improved this paper.

REFERENCES

Abazajian et al. 2009, ApJS, submitted (DR7)
Adelman, S. J., & Gulliver, A. F., 1990, ApJ, 348, 712
Adelman-McCarthy, J. K., et al., 2008, ApJS, 175, 297
Aufdenberg, J. P., et al., 2006, ApJ, 645, 664
Althaus, L. G., García-Berro, E., Isern, J., & Córsico, A. H., 2005, A&A, 441, 689
Auer, L., 2003, Stellar Atmosphere Modeling, ASP Conf. Proceedings, Vol 288, p.3, San Francisco
Barstow, M. A., Good, S. A., Burleigh, M. R., Hubeny, I., Holberg, J. B., & Levan, A. J., 2003a, MNRAS, 344, 562
Barstow, M. A., Good, S. A., Holberg, J. B., Hubeny, I., Bannister, N. P., Bruhweiler, F. C., Burleigh, M. R., & Napiwotzki, R., 2003b, MNRAS, 341, 870
Barstow, M. A., Holberg, J. B., Hubeny, I., Good, S. A., Levan, A. J., & Meru, F., 2001, MNRAS, 328, 211
Barstow, M. A., Hubeny, I., & Holberg, J. B., 1998, MNRAS, 299, 520
Bergeron, P., Saffer, R. A., & Liebert, J., 1992, ApJ, 394, 228
Bohlin, R. C., 1996, AJ, 111, 1743
Bohlin, R. C., 2000, AJ, 120, 437
Bohlin, R. C. 2007, The Future of Photometric, Spectrophotometric and Polarimetric Standardization, ASP Conf. Proceedings, Vol. 364, p. 315, San Francisco
Bohlin, R. C., Colina, L., & Finley, D. S., 1995, AJ, 110, 1316
Bohlin, R. C., Dickinson, M. E., & Calzetti, D. 2001, AJ, 122, 2118
Bohlin, R. C., & Gilliland, R. L., 2004, AJ, 128, 3053
DeGennaro, S., von Hippel, T., Winget, D. E., Kepler, S. O., Nitta, A., Koester, D., & Althaus, L., 2008, AJ, 135, 1
Dixon, W. V., et al., 2007, PASP, 119, 527
Eisenstein, D. J., et al., 2006, ApJS, 167, 40
Finley, D. S., Basri, G., & Bowyer, S., 1990, ApJ, 359, 483
Finley, D. S., Koester, D., & Basri, G., 1997, ApJ, 488, 375
Fitzpatrick, E. L., 1999, PASP, 111, 63
García-Gil, A., García López, R. J., Allende Prieto, C., & Hubeny, I., 2005, ApJ, 623, 460
Goudfrooij, P., Bohlin, R. C., Maíz-Apellániz, J., & Kimble, R. A., 2006, PASP, 118, 1455
Holberg, J. B., Ali, B., Carone, T. E., & Polidan, R. S., 1991, ApJ, 375, 716
Harris, H. C., et al., 2003, AJ, 126, 1023
Holberg, J. B., & Bergeron, P., 2006, AJ, 132, 1221
Holberg, J. B., Bergeron, P., & Gianninas, A., 2008, AJ, 135, 1239
Holberg, J. B., Forrester, W. T., Shemansky, D. E., & Barry, D. C., 1982, ApJ, 257, 656
Homeier, D., Koester, D., Hagen, H.-J., Jordan, S., Heber, U., Engels, D., Reimers, D., & Dreizler, S., 1998, A&A, 338, 563
Hubeny, I., Hummer, D. G., & Lanz, T., 1994, A&A, 282, 151
Hubeny, I., & Lanz, T., 1995, ApJ, 439, 875
Ivezić, Ž., et al., 2007, AJ, 134, 973
Kepler, S. O., Kleinman, S. J., Nitta, A., Koester, D., Castanheira, B. G., Giovannini, O., Costa, A. F. M., & Althaus, L., 2007, MNRAS, 375, 1315
Kilic, M., Allende Prieto, C., Brown, W. R., & Koester, D., 2007, ApJ, 660, 1451
Kleinman, S. J., et al., 2004, ApJ, 607, 426
Koester, D., et al., 2001, A&A, 378, 556

Kruk, J. W., Brown, T. M., Davidsen, A. F., Espey, B. R., Finley, D. S., & Kriss, G. A., 1999, ApJS, 122, 299
Landolt, A. U., 1992, AJ, 104, 340
Lanz, T., Barstow, M. A., Hubeny, I., & Holberg, J. B., 1996, ApJ, 473, 1089
Lanz, T., & Hubeny, I. 1995, ApJ, 439, 905
Laureijs, R. J., Jourdain de Muizon, M., Leech, K., Siebenmorgen, R., Dominik, C., Habing, H. J., Trams, N., & Kessler, M. F., 2002, A&A, 387, 285
Lemke, M., 1997, A&AS, 122, 285
Liebert, J., Bergeron, P., & Holberg, J. B., 2005, ApJS, 156, 47
Marsh, M. C., et al., 1997, MNRAS, 287, 705
Nelder, J. & Mead, R. 1965, Computer Journal, 7, 308
Oke, J. B., & Gunn, J. E., 1983, ApJ, 266, 713
Pérez Hernández, F., Claret, A., Hernández, M. M., & Michel, E., 1999, A&A, 346, 586
Ramírez, I., Allende Prieto, C., Redfield, S., & Lambert, D. L., 2006, A&A, 459, 613
Rider, C. J., Tucker, D. L., Smith, J. A., Stoughton, C., Allam, S. S., & Neilsen, E. H., Jr., 2004, AJ, 127, 2210
Schlegel, D. J., Finkbeiner, D. P., & Davis, M., 1998, ApJ, 500, 525
Sing, D., Holberg, J. B., & Dupuis, J., 2002, Continuing the Challenge of EUV Astronomy: Current Analysis and Prospects for the Future, 264, 57
Smith, J. A., et al., 2002, AJ, 123, 2121
Stoughton, C., et al. 2002, AJ, 123, 485 (EDR)
Thakar, A. R. Szalay, A., Fekete, G., & Gray, J., 2008, Computing in Science and Engineering, 10, 1 (Jan/Feb 2008), 30
Tucker, D. L., et al., 2006, Astronomische Nachrichten, 327, 821

APPENDIX A: USNO $U'G'R'I'Z'$ PHOTOMETRY FOR THE HST STANDARDS

The observations were obtained using the 1.0-m Ritchey–Chrétien telescope at the U.S. Naval Observatory's Flagstaff Station (USNO-FS) during the bright time between October 2005 and April 2006. The detector was a thinned, UV-AR coated, Tektronix TK1024 CCD with a gain of 7.43±0.41 e^- and a read-noise of 6.0 e^-. This CCD is similar to the CCDs used in the main SDSS survey camera and the CCD used by the 0.5-m photometric monitoring telescope at APO. The camera scale of 0.68 arcsec/pixel produced a field of view of 11.54 arcmin.

The five filters of the $u'g'r'i'z'$ system have effective wavelengths of 3540 Å, 4750 Å, 6222 Å, 7632 Å, and 9049 Å, respectively, at 1.2 airmasses (Fukugita et al. 1996; note that the g' filter has been determined to have an effective wavelength 20 Å bluer than that originally quoted). The filter transmission data as measured by the Japan Participation Group within the SDSS, and the CCD+filter response curves updated by J. Gunn in 2001 are available on-line[7]. We refer the reader to Smith et al. 2002 for more details about the observations, and to Smith et al. 2007 for a historical description of the SDSS photometric system.

All the individual measurements are given in Table A. About 9, 4 and 12 observations were obtained for G191 B2B, GD 153 and GD 71, respectively. The exposure times were (in order $u'g'r'i'z'$) 60, 15, 15, 40, 90 s for G191 B2B, 100, 25, 25, 60, 130 s for GD 153, and 20, 8, 10, 12, 50 for GD 71. The average $u'g'r'i'z'$ magnitudes from the USNO 1.0-m, included in Table A, were converted to the SDSS 2.5-m *ugriz* system using the Equations 2–6 in Tucker et al. 2006[8]. We note that the transformations were derived from stars cooler than our standards. Rider et al. (2004) found that they are still adequate for colors bluer than originally defined, although still far from the extremely blue colors of the white dwarfs considered in this paper ($u - g < -0.3$). The derived *ugr* magnitudes are included in Table 5.

[7] `http://www-star.fnal.gov/ugriz/Filters/response.html`

[8] Also given at http://www.sdss.org/dr7/algorithms/jeg_photometric_eq_dr1.ht

Table A1. Photometry for the HST standards in the USNO $u'g'r'i'z'$ bandpasses.

MJD ≡ JD -240,000,000.5 (days)	u' (mag)	g' (mag)	r' (mag)	i' (mag)	z' (mag)
		G 191 B2B			
53650	11.006	11.517	12.034	12.419	12.739
53651	11.024	11.533	12.046	12.421	12.754
53654	11.011	11.513	12.019	12.402	12.713
53685	11.028	11.525	12.049	12.425	12.739
53687	11.035	11.523	12.032	12.422	12.710
53702	11.006	11.524	12.035	12.410	12.731
53714	11.017	11.511	12.025	12.403	12.735
53715	11.017	11.513	12.039	12.419	12.734
53740	...	11.519	12.025	12.406	12.732
Mean	11.018	11.520	12.034	12.414	12.732
Std. Dev.	0.011	0.007	0.010	0.009	0.013
Std. Err.	0.004	0.002	0.003	0.003	0.005
		GD 153			
53797	12.695	13.132	13.615	13.974	14.304
53832	12.701	13.125	13.611	13.972	14.260
53833	12.704	13.121	13.611	13.968	14.300
53850	12.700	13.123	13.610	13.982	14.290
Mean	12.700	13.125	13.612	13.974	14.289
Std. Dev.	0.004	0.005	0.002	0.006	0.020
Std. Err.	0.002	0.002	0.001	0.003	0.010
		GD 71			
53650	12.422	12.814	13.274	13.646	13.973
53650	12.426	...	13.279	...	13.987
53651	12.451	12.819	13.282	13.656	13.979
53654	12.438	12.809	13.271	13.634	13.962
53687	12.457	12.819	13.284	13.652	13.965
53702	12.423	12.802	13.274	13.644	13.948
53714	12.443	12.799	13.274	13.637	13.967
53715	12.447	12.820	13.283	13.650	13.966
53740	12.444	12.812	13.277	13.639	13.958
53742	12.462	12.822	13.295	13.667	13.963
53832	12.451	12.828	13.286	13.645	13.976
53833	12.445	12.818	13.275	13.651	13.959
Mean	12.442	12.815	13.280	13.647	13.967
Std. Dev.	0.013	0.009	0.007	0.009	0.011
Std. Err.	0.004	0.003	0.002	0.003	0.003